Letter

# Photon-mediated correlated hopping in a synthetic ladder

Anjun Chu,[1,2,*] Asier Piñeiro Orioli,[1,2] Diego Barberena,[1,2] James K. Thompson,[1] and Ana Maria Rey[1,2]
[1]*JILA, NIST and Department of Physics, University of Colorado, Boulder, Colorado 80309, USA*
[2]*Center for Theory of Quantum Matter, University of Colorado, Boulder, Colorado 80309, USA*

(Received 5 August 2022; revised 9 February 2023; accepted 5 May 2023; published 17 May 2023)

We propose a different direction in quantum simulation that uses multilevel atoms in an optical cavity as a toolbox to engineer different types of bosonic models featuring correlated hopping processes in a synthetic ladder spanned by atomic ground states. The underlying mechanisms responsible for correlated hopping are collective cavity-mediated interactions that dress a manifold of excited levels in the far-detuned limit. By weakly coupling the ground-state levels to these dressed states using two laser drives with appropriate detunings, one can engineer correlated hopping processes while suppressing undesired single-particle and collective shifts of the ground-state levels. We discuss the rich many-body dynamics that can be realized in the synthetic ladder including pair production processes, chiral transport, and light-cone correlation spreading. The latter illustrates that an effective notion of locality can be engineered in a system with fully collective interactions.

DOI: 10.1103/PhysRevResearch.5.L022034

## I. INTRODUCTION

Correlated hopping, a process whereby the hopping rate of a particle depends on the presence of other particles in an array, is believed to contribute to the complex behaviors seen in strongly correlated materials [1–3], and also to be a key requisite for the generation of dynamical gauge fields [4,5] and topological behaviors [6,7]. Regardless of its importance, correlated hopping is typically small and hard to manipulate in real materials, and ultracold atoms have been identified as a unique playground to study these processes under controllable conditions. However, the implementation so far has been mainly limited to isolated double-well arrays [4,5], indirect detection via spectroscopic measurements [8–11], or weak corrections due to dipolar interaction of magnetic atoms [12]. Experimentally accessible protocols to engineer correlated hopping processes in strongly interacting many-body systems are still lacking.

In this work, we propose the use of multilevel atoms in an optical cavity as a toolbox to engineer different types of bosonic models featuring correlated hopping processes in a genuine unitary many-body system. Cavity QED systems have started to demonstrate their great potential as quantum simulators [13–26]. Important initial steps for correlated hopping have been achieved such as the engineering of pair production processes [17,22] and dissipative dynamical tunneling [24]. Therefore, the time is ripe to explore the full power of cavity systems under accessible conditions.

A key idea behind our protocol is to treat the internal levels of the atoms as a synthetic dimension [27], where a notion of spatial locality can naturally emerge, even in the presence of infinite-range photon-mediated interactions. The use of internal levels as a synthetic spatial dimension has already led to beautiful demonstrations of topological lattice models and chiral transport in noninteracting systems [28–32], and very recently in interacting many-body systems [33]. Here, we propose a way to go beyond the single-particle paradigm by engineering interaction-induced hopping processes in the synthetic dimension spanned by the atomic ground-state manifold. This is accomplished by weakly coupling it to a set of many-body excited states dressed by photon-mediated interactions.

The implementation uses two laser drives with appropriate detunings to suppress undesirable single-particle and collective shifts of the internal levels. In this way, we energetically favor only the desired hopping process where in a correlated manner one atom moves *two* internal levels up while another atom in the array moves *two* levels down. The correlated hopping processes we introduce split the ground-state manifold into two sets of levels, which we visualize as a synthetic two-leg ladder. By doing that, we open up a variety of many-body phenomena that can be realized in this system, including dynamical phase transitions in pair production processes, chiral transport tunable via laser detunings and initial state preparation, and correlation spreading and emergent light-cone transport in the synthetic ladder. We also discuss a feasible experimental implementation using long-lived alkaline-earth atoms.

## II. SYSTEM

### A. Effective Hamiltonian

We consider an ensemble of $N$ multilevel atoms confined in an optical cavity with quantization axis ($\hat{z}$) along the cavity

*anjun.chu@colorado.edu

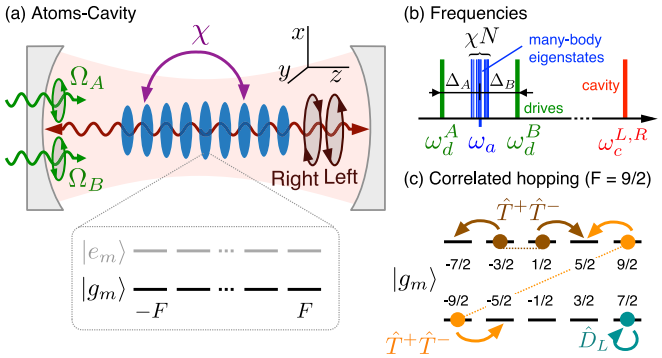


FIG. 1. Effective ground-state dynamics in a multilevel cavity QED system. (a) An ensemble of multilevel atoms (blue pancakes) with ground ($|g_m\rangle$) and excited ($|e_m\rangle$) manifold are trapped in an optical cavity with quantization axis ($\hat{z}$) along the cavity axis. The cavity photons (red curve) with left-handed ($\sigma^-$) and right-handed ($\sigma^+$) circular polarizations mediate collective interactions ($\chi$) among the atoms. Two external drives are applied to the $\sigma^-$ polarized mode with atomic Rabi frequency $\Omega_{A,B}$. (b) Frequencies of cavity resonance, two external drives, and atomic transition dressed by photon-mediated interactions. (c) Sketch of the correlated hopping ($\hat{T}^+\hat{T}^-$) and single-particle ac Stark shifts ($\hat{D}_L$) in the synthetic two-leg ladder spanned by the ground manifold ($|g_m\rangle$), using $F = \frac{9}{2}$ case as an example.

axis, as depicted in Figs. 1(a) and 1(b). The internal level structure of each atom consists of a ground and an excited manifold with hyperfine spin $F_g$ and $F_e$, respectively. The excited-state manifold decays with spontaneous emission rate $\gamma$. We consider a weak magnetic field limit such that all atomic transition frequencies can be approximated as a single $\omega_a$ [34]. Specifically, we label the ground states as $|g_m\rangle_i$, and the excited states as $|e_m\rangle_i$, where $m$ is the magnetic quantum number, and $i$ labels the atoms. Two degenerate cavity modes with left-handed ($\sigma^-$) and right-handed ($\sigma^+$) circular polarization at frequency $\omega_c \equiv \omega_c^{L,R}$ couple to the transition between ground and excited manifolds with coupling strength $g_c$ and detuning $\Delta_c = \omega_c - \omega_a$. Two external $\sigma^-$ polarized lasers with frequencies $\omega_d^{A,B}$, detuned from the atomic transition by $\Delta_{A,B} = \omega_d^{A,B} - \omega_a$, are used to drive the cavity with intracavity Rabi frequency $\Omega_{A,B}$, respectively.

We focus on the far-detuned regime of the cavity ($|\Delta_c| \gg |\Delta_{A,B}|$), where the frequencies of laser drives are closer to the atomic transition rather than the cavity resonance. In this regime, one can first adiabatically eliminate the injected light fields and intracavity fluctuations assuming $|\Delta_c| \gg g_c\sqrt{N}, \kappa$, with $\kappa$ the cavity intensity decay rate. The system is thus well described by an atom-only Hamiltonian with photon-mediated elastic interactions [34,35]

$$\hat{H}/\hbar = \omega_a \hat{N}_e + \chi(\hat{L}^+\hat{L}^- + \hat{R}^+\hat{R}^-) + \left[\left(\Omega_A e^{-i\omega_d^A t} + \Omega_B e^{-i\omega_d^B t}\right)\hat{L}^+ + \text{H.c.}\right], \quad (1)$$

where $\chi = -g_c^2/\Delta_c$ is the photon-mediated interaction strength. Here, $\hat{N}_e = \sum_{im} |e_m\rangle\langle e_m|_i$ is the atom number operator for the excited manifold, $\hat{L}^+ = \sum_{im} C_m^{-1} |e_{m-1}\rangle\langle g_m|_i$, $\hat{L}^- = (\hat{L}^+)^\dagger$ are multilevel dipole operators with $\sigma^-$ polarization, and $\hat{R}^+ = \sum_{im} C_m^{+1} |e_{m+1}\rangle\langle g_m|_i$, $\hat{R}^- = (\hat{R}^+)^\dagger$ are multilevel dipole operators with $\sigma^+$ polarization, where $C_m^p \equiv \langle F_g, m; 1, p | F_e, m+p\rangle$ are the Clebsch-Gordan coefficients.

The photon-mediated interactions in $\hat{H}$ [Eq. (1)] exchange excitations among atoms and generate a rich many-body spectrum of collective states [see Fig. 1(b)], if $|\chi N| \gg \gamma$. In this regime and assuming weak driving fields ($|\Delta_{A,B}|, |\chi N| \gg |\Omega_{A,B}|$), as shown in [34], the many-body excited states are only virtually populated and can be adiabatically eliminated, giving rise to net interactions in the atomic ground manifold described by the following effective ground-state Hamiltonian:

$$\hat{H}_{\text{eff}}/\hbar = \sum_{\nu=A,B} \frac{|\Omega_\nu|^2 \Delta_\nu}{\chi} \left[\Delta_\nu - \chi \hat{D}_L - \chi^2 \hat{T}^+ \hat{G}_R^\nu \hat{T}^-\right]^{-1}, \quad (2)$$

where $\hat{G}_R^\nu = (\Delta_\nu - \chi \hat{D}_R)^{-1}$. Here, $\hat{D}_L = \hat{P}_g \hat{L}^- \hat{L}^+ \hat{P}_g$, $\hat{D}_R = \hat{P}_g \hat{R}^- \hat{R}^+ \hat{P}_g$, $\hat{T}^+ = \hat{P}_g \hat{L}^- \hat{R}^+ \hat{P}_g$, and $\hat{T}^- = (\hat{T}^+)^\dagger$ are operators acting only on the ground manifold as ensured by $\hat{P}_g$, which is defined as the projection operator of the atomic ground states. In the case of $F_g = F_e = F$ as we explore in this paper, these operators can be expressed as $\hat{D}_{L,R} = \sum_i \hat{D}_i^{L,R}/\mathcal{N}_F$ and $\hat{T}^+ = \sum_i \hat{T}_i^+/\mathcal{N}_F$, where

$$\hat{D}_i^L = \hat{S}_i^+ \hat{S}_i^-, \quad \hat{D}_i^R = \hat{S}_i^- \hat{S}_i^+, \quad \hat{T}_i^+ = -\hat{S}_i^+ \hat{S}_i^+, \quad (3)$$

$\mathcal{N}_F = 2F(F+1)$ is the normalization factor, and $\hat{S}_i^\pm$ are raising and lowering spin-$F$ operators acting on atom $i$. Note that $\hat{H}_{\text{eff}}$ is fully collective and thus couples an atom $i$ with any other atom $j$ in the ensemble. If the atoms start in the permutationally symmetric manifold, or on a direct product state of permutationally symmetric subsystems, they will remain there, and the scaling of Hilbert space dimension with atom number $N$ is reduced from exponential to polynomial. Thanks to this simplification, we perform all the numerical calculations using Eq. (2). However, the underlying physics in $\hat{H}_{\text{eff}}$, which includes a sum over multibody interactions, is still extremely complex even in this restricted Hilbert space.

### B. Discussions

To gain physical intuition of the physical processes encapsulated in Eq. (2), first we discuss the simplest case with $F = \frac{1}{2}$, which gives $\hat{T}^\pm = 0$, and $\hat{D}_L = 2(N/2 + \hat{S}_z)/3$. So the effective ground-state Hamiltonian takes the form

$$H_{\text{eff}}/\hbar = \sum_{\nu=A,B} \frac{|\Omega_\nu|^2 \Delta_\nu/\chi}{\Delta_\nu - 2\chi(N/2 + \hat{S}_z)/3}. \quad (4)$$

In the off-resonant regime ($|\Delta_{A,B}| \gtrsim |\chi N|$), one can expand $\hat{H}_{\text{eff}}$ in a power series of the $\hat{S}_z$ operator. At the leading nontrivial order, this expansion recovers the well-known one-axis twisting interaction $\hat{S}_z\hat{S}_z$, a powerful resource for spin-squeezing generation [36]. At higher orders it also generates non-negligible $n$-body interaction terms such as $(\hat{S}_z)^n$ when $\Delta_{A,B}$ is comparable with $\chi N$. Such multibody operators, which emerge naturally in our system, can speed up the entanglement generation dynamics as recently suggested in trapped ion arrays [37].

In the presence of more levels ($F > \frac{1}{2}$), the operators $\hat{T}^\pm$ cannot be ignored and they start to play a nontrivial role, leading to tunable multibody interactions. Regardless of their

complexity, one can gain physical insight by focusing on the leading-order terms obtained in a power series in $\chi N/\Delta_{A,B}$. To leading order the effective Hamiltonian simplifies to

$$\hat{H}_{\rm eff}/\hbar \approx \sum_{\nu=A,B} \frac{|\Omega_\nu|^2}{\Delta_\nu}\hat{D}_L + \frac{|\Omega_\nu|^2\chi}{\Delta_\nu^2}(\hat{D}_L\hat{D}_L + \hat{T}^+\hat{T}^-). \quad (5)$$

The first term in Eq. (5) describes single-particle ac Stark shifts generated by each light field injected into the cavity, and the second term describes the leading-order interactions in the ground manifold generated by exchanging cavity photons. The exchange of $\sigma^-$ polarized cavity photon leads to the diagonal $\hat{D}_L\hat{D}_L$ term, a multilevel generalization of one-axis twisting interaction, generating population-dependent collective shifts on the ground-state levels. In contrast, the exchange of $\sigma^+$ polarized cavity photon leads to the $\hat{T}^+\hat{T}^-$ term, a new term emerged in multilevel ground states, generating the processes where one atom moves two internal levels down ($\hat{T}^-$) while another atom moves two levels up ($\hat{T}^+$).

Assuming the hyperfine spin $F$ is a half-integer, it is convenient to visualize the atomic ground manifold as a synthetic two-leg ladder, where the upper and lower legs are sets of internal states directly connected by the $\hat{T}^\pm$ operators [see Fig. 1(c)]. Under this concept, the $\hat{T}^+\hat{T}^-$ term is equivalent to correlated hopping in the synthetic ladder which can occur between atoms in the same leg or in different legs. These processes can generate strong correlations between the legs despite having no direct hopping processes.

In order to better understand the Hamiltonian dynamics, it is useful to write the operators acting only on the ground manifold in terms of Schwinger bosons,

$$\hat{D}_L = \sum_m \left(C_m^{-1}\right)^2 \hat{a}_m^\dagger \hat{a}_m, \quad \hat{D}_R = \sum_m \left(C_m^{+1}\right)^2 \hat{a}_m^\dagger \hat{a}_m,$$
$$\hat{T}^+ = \sum_m C_m^{+1} C_{m+2}^{-1} \hat{a}_{m+2}^\dagger \hat{a}_m, \quad (6)$$

where $\hat{a}_m$ is the bosonic annihilation operator for state $|g_m\rangle$. For simplicity, we also set the strength of the external drives to $\Omega \equiv \Omega_{A,B} = 0.05\chi N$, and analyze the unitary dynamics by varying the detunings $\Delta_{A,B}$ of the laser drives. By appropriate choices of $\Delta_{A,B}$, we can suppress the single-particle and collective shifts at $t = 0$, and make the correlated hopping terms as the dominant process in the synthetic ladder [34].

## III. EXAMPLES OF CORRELATED HOPPING

### A. Pair production

One of the simplest cases to understand the correlated hopping process ($\hat{T}^+\hat{T}^-$) is a system with a four-level $F = \frac{3}{2}$ ground-state manifold [see Fig. 2(a)]. Considering the initial state $|g_{-3/2}\rangle^{\otimes(N/2)}|g_{3/2}\rangle^{\otimes(N/2)}$, the role of the $\hat{T}^+\hat{T}^-$ term is to generate correlated atom pairs in the initially unoccupied states $|g_{-1/2}\rangle$ and $|g_{1/2}\rangle$. We show that $\hat{H}_{\rm eff}$ [Eq. (2)] in this system features an abrupt change of dynamical behavior as we tune the system parameters, i.e., dynamical phase transition (DPT). This type of DPT generated by pair production processes can be analyzed at both short times and long times [38].

The short-time dynamics can be understood via undepleted pump approximation (UPA), where to the leading order one

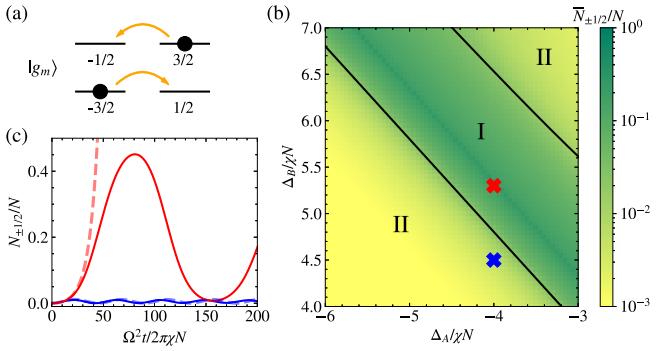


FIG. 2. Pair production dynamics in a synthetic four-level ladder. (a) The black dots show the initial state of the atoms and the orange arrows show the correlated hopping process. (b) Dynamical phase diagram of pair production process. The black lines are the phase boundary separating phase I (with pair production) and phase II (without pair production). (c) Short-time dynamics in phase I (red curves) and phase II (blue curves). The choices of detunings $\Delta_{A,B}$ are indicated by cross marks in (b) with corresponding color. The solid lines are calculated by exact diagonalization (ED), while the dashed lines are based on undepleted pump approximation (UPA).

can replace the bosonic operators for macroscopically occupied states as $c$ numbers, $\hat{a}_{\pm3/2}, \hat{a}_{\pm3/2}^\dagger \sim \sqrt{N/2}$. Under UPA, $\hat{H}_{\rm eff}$ [Eq. (2)] becomes quadratic and therefore can be diagonalized analytically:

$$\hat{H}_{\rm eff}/\hbar \approx K_1\hat{a}_{-1/2}^\dagger\hat{a}_{-1/2} + K_2\hat{a}_{1/2}^\dagger\hat{a}_{1/2} + K_3(\hat{a}_{-1/2}\hat{a}_{1/2} + \text{H.c.}). \quad (7)$$

Here, $K_1$, $K_2$, and $K_3$ can be expressed as functions of $\Delta_{A,B}/\chi N$ [34]. The term proportional to $K_3$ is responsible for generating correlated atom pairs, while the terms proportional to $K_{1,2}$ impose an energy penalty for the pair production. Note that Eq. (7) is equivalent to the two-mode squeezing Hamiltonian well known in quantum optics [39] and spinor BEC systems [36,40], and very recently achieved in cavity QED systems [17,22]. At short times when UPA is valid [see Fig. 2(c)], one observes exponential growth of atom population $N_{\pm1/2}$ in the initially unoccupied states $|g_{\pm1/2}\rangle$ (red curves) in phase I (with pair production), which is described by $(K_1 + K_2)^2 < 4K_3^2$. Instead in phase II (without pair production), described by $(K_1 + K_2)^2 > 4K_3^2$, one observes small oscillations of atom population (blue curves). The dynamical critical points are located at $(K_1 + K_2)^2 = 4K_3^2$ [see black lines in Fig. 2(b)].

To analyze the dynamics generated by $\hat{H}_{\rm eff}$ [Eq. (2)] at longer times, we use exact diagonalization (ED) with 100 atoms. At long times the DPT is signaled by a sharp change in behavior of the long-time average fractional population $\overline{N}_{\pm1/2}/N = \lim_{T\to\infty}\int_0^T dt\, N_{\pm1/2}(t)/(NT)$, which serves as an order parameter and distinguishes the two dynamical phases [see Fig. 2(b)]. Phase I is characterized by nonzero $\overline{N}_{\pm1/2}/N$, while phase II is characterized by $\overline{N}_{\pm1/2}/N \approx 0$. We analyze the critical exponents of this DPT in [34]. Our discussions of the four-level system can be generalized to larger synthetic ladders directly, and the detunings $\Delta_{A,B}$ serve as control knobs of the correlated hopping process.

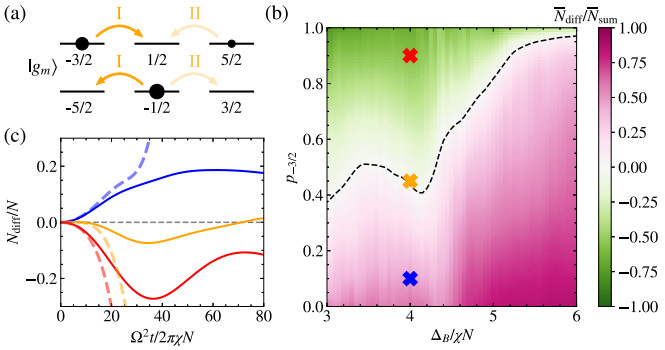


FIG. 3. Chiral transport in a synthetic six-level ladder. (a) The strength of the relevant correlated hopping processes (orange arrows) is indicated by the opacity of the arrows, which depends on the atom distribution in the upper leg (black dots). (b) Chiral transport behavior in the lower leg depends on the initial probability of occupying the state $|g_{-3/2}\rangle$ ($y$ axis) and the detuning of the external drive $B$ ($x$ axis) for fixed drive $A$ detuning which is set to $\Delta_A = -3\chi N$. The dashed line indicates balanced transport. (c) Short-time dynamics of population imbalance with parameters indicated by cross marks in (b) using the same color. The solid lines are calculated by ED, while the dashed lines are based on UPA.

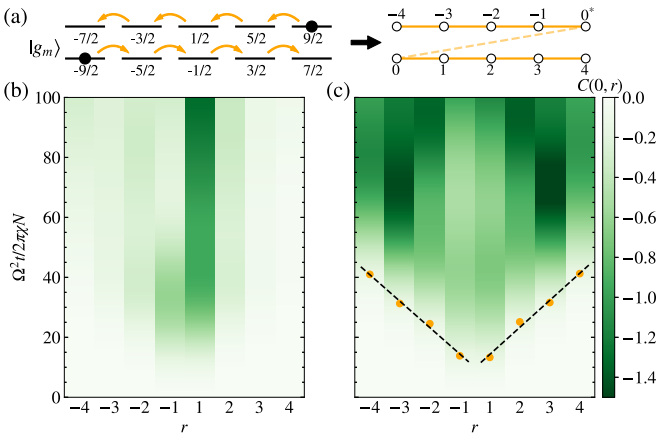


FIG. 4. Correlation spreading in a synthetic 10-level ladder. (a) The correlated hopping processes (orange arrows) for the initial state (black dots) allow us to assign position indices based on the direction of hopping. The orange dashed line indicates the spread of correlations between legs without direct hopping processes. (b) The atom number two-point correlations (see text) are restricted to nearest-neighbor sites for $\Delta_A = -3\chi N$, $\Delta_B = 3.7\chi N$, (c) but can undergo light-cone spreading for $\Delta_A = -3\chi N$, $\Delta_B = 4.1\chi N$.

### B. Chiral transport

Including more levels in the dynamics opens up the possibility to engineer interaction-induced chiral transport. As shown in Fig. 3(a), this can be achieved in a six-level model ($F = \frac{5}{2}$) by preparing atoms in the $|g_{-1/2}\rangle$ state, which is the center of the lower leg. The chiral transport in the lower leg can be characterized by the population difference between atoms hopping to the right side ($|g_{3/2}\rangle$) and the left side ($|g_{-5/2}\rangle$), $N_{\rm diff} = N_{3/2} - N_{-5/2}$. The chiral transport is not a consequence of the external drive polarization. Suppose there are no atoms in the upper leg: the only relevant correlated hopping process will generate atom pairs in the state $|g_{-5/2}\rangle$ and $|g_{3/2}\rangle$, which leads to $N_{\rm diff} = 0$. Nevertheless, adding atoms in the upper chain gives rise to extra correlated hopping processes, in which the processes I and II shown in Fig. 3(a) become the dominant processes and break left-right symmetry at short time [34]. If process I is stronger than process II, we have chiral transport to the left side of the lower chain ($N_{\rm diff} < 0$), and vice versa.

We analyze the chiral transport behavior via ED of $\hat{H}_{\rm eff}$ [Eq. (2)] with 20 atoms. The initial state of this calculation is $[\sqrt{p_{-3/2}}|g_{-3/2}\rangle + \sqrt{1-p_{-3/2}}|g_{5/2}\rangle]^{\otimes(N/2)}|g_{-1/2}\rangle^{\otimes(N/2)}$, where $p_{-3/2}$ is the initial probability of occupying the state $|g_{-3/2}\rangle$ for the atoms in the upper leg. The normalized long-time average $\overline{N}_{\rm diff}/\overline{N}_{\rm sum}$ as a function of $p_{-3/2}$ and $\Delta_B$, where $N_{\rm sum} = N_{3/2} + N_{-5/2}$, is shown in Fig. 3(b) for fixed $\Delta_A$. It can be seen that for different choices of $\Delta_B$ it is possible to turn on both processes (I and II) if $\Delta_B/\chi N \in (3,4)$, or mainly turn on process II if $\Delta_B/\chi N \in (5,6)$. Enforcing balanced transport [see the dashed line in Fig. 3(b)] requires equal weight of processes I and II in the former case, or suppression of both processes in the latter case. In Fig. 3(c), we compare the short-time dynamics of chiral transport at $\Delta_B = 4\chi N$ with different choices of $p_{-3/2}$, indicating that the transport direction is fully tunable via initial state in this case. Unlike the four-level system discussed above, UPA is not able to provide a qualitative description of chiral transport behavior at long times.

### C. Correlation spreading

Regardless of the all-to-all nature of the cavity-mediated interactions, in our synthetic ladder we can engineer light-cone spreading of quantum correlations analogous to the one observed in real lattices with short-range or power-law interactions [41–43]. In Fig. 4(a), we show a 10-level $F = \frac{9}{2}$ ground-state manifold visualized as a synthetic ladder. For an initial product state $|g_{-9/2}\rangle^{\otimes(N/2)}|g_{9/2}\rangle^{\otimes(N/2)}$, it is possible to visualize the correlation spreading from a concatenated set of hopping processes [see orange arrows in Fig. 4(a)] by assigning position indices for the synthetic lattice sites: 0 and $0^*$ for the initial sites, and site labels increasing to the right and decreasing to the left. Using this convention, we can analyze the correlation spreading in our synthetic ladder, in terms of the two-point correlators $C(i,j) = \langle \hat{N}_i \hat{N}_j \rangle - \langle \hat{N}_i \rangle \langle \hat{N}_j \rangle$.

For the case of a system of 10 atoms, ED of $\hat{H}_{\rm eff}$ [Eq. (2)] shows two distinct behaviors of $C(0,r)$ depending on the choice of $\Delta_B$ for fixed $\Delta_A$. In one parameter regime, differential energy shifts imposed by $\Delta_B$ favor localization and the correlation is restricted to nearest-neighbor sites [see Fig. 4(b)]; for another configuration, linear correlation spreading ($t \propto r$) to the whole system is energetically allowed [see Fig. 4(c)]. The spreading is signaled by the appearance of a symmetric light cone [orange points in Fig. 4(c)] in the two-point correlators, which is set at the time when $C(0,r)$ reaches $-0.15$ ($\sim$10% of the maximum value).

## IV. EXPERIMENTAL IMPLEMENTATION

Our protocol can be directly implemented using fermionic alkaline-earth atoms featuring $F_g > 0$ in a cavity. The main

advantage of these atoms is their unique atomic structure which offers simple ground- ($^1S_0$) and long-lived excited-state manifolds (e.g., $^3P_1$) where we can explicitly isolate a single $F_g \to F_e$ transition, such as $\frac{5}{2} \to \frac{5}{2}$ for $^{173}$Yb and $\frac{9}{2} \to \frac{9}{2}$ for $^{87}$Sr. Although it might be possible to engineer similar correlated hopping processes in the ground hyperfine levels of alkali atoms, the proposed implementation is less direct since in this system the condition $|\chi N| \gg \gamma$ requires to make $\chi N$ comparable to the excited hyperfine splitting and as a consequence it is necessary to sum over the set of all excited hyperfine levels. For the particular case of $^{87}$Sr as discussed in [34], under current experimental conditions it is possible to operate in a regime where $|\chi N|/\gamma > 10^2$ using $2\times10^5$ atoms, so the dissipation during the timescale of interests can be ignored. Moreover, our protocol can be directly generalized to the case with inhomogeneous atom-cavity couplings $g_i = g_c\eta_i$. The effective ground-state Hamiltonian [Eq. (2)] still takes the same form if we redefine the operators in Eq. (3) as $\hat{D}_i^L = \eta_i^2\hat{S}_i^+\hat{S}_i^-$, $\hat{D}_i^R = \eta_i^2\hat{S}_i^-\hat{S}_i^+$, $\hat{T}_i^+ = -\eta_i^2\hat{S}_i^+\hat{S}_i^+$ [34].

The most common type of initial state required in our protocol, $|g_{-F}\rangle^{\otimes(N/2)}|g_F\rangle^{\otimes(N/2)}$, has already been demonstrated in previous experiments using $^{87}$Sr atoms [16,44]. It is achieved by targeting the $|g_{\pm F}\rangle$ states to be dark states of a laser-cooling process. The generated state has roughly equal number of atoms in these two levels with no initial coherence, up to a statistical atom number imbalance in the order of $\sqrt{N}$. The small imbalance in the prepared state has negligible effects on the physical phenomena we are investigating, for the large ensemble situations relevant for current cavity QED experiments.

## V. CONCLUSION AND OUTLOOK

We have presented a protocol to explore correlated hopping processes using cavity-mediated interactions and discussed a few examples in regimes tractable by current theoretical methods. However, even in the permutationally symmetric subspace, more generic initial conditions can lead to situations only explorable directly in experiments. Moreover, with additional tuning knobs currently accessible in experiments we open further opportunities for quantum simulation. For example, using an additional transverse magnetic field, our protocol opens a path to engineer dynamical gauge fields since the hopping phase in correlated hopping processes can be dynamically adjusted by the presence of other particles. Furthermore, even though here we assume a dilute gas and ignore contact interactions between atoms, by trapping atoms in 3D optical lattices, it is possible to make superexchange interactions comparable to the correlated hopping strength, opening a path for designing complex many-body Hamiltonians that are likely to display fast scrambling of quantum information and chaotic quantum behaviors [45].

## ACKNOWLEDGMENTS

We thank A. Friedman and T. Bothwell for useful discussions. This work is supported by the AFOSR Grant No. FA9550-18-1-0319, by the DARPA (funded via ARO) Grant No. W911NF-16-1-0576, the ARO single investigator Grant No. W911NF-19-1-0210, the NSF Grants No. PHY1820885, No. JILA-PFC PHY-1734006, and No. QLCI-2016244, by the DOE Quantum Systems Accelerator (QSA) grant, and by NIST.

[1] O. Dutta, M. Gajda, P. Hauke, M. Lewenstein, D.-S. Lühmann, B. A. Malomed, T. Sowiński, and J. Zakrzewski, Non-standard hubbard models in optical lattices: A review, Rep. Prog. Phys. **78**, 066001 (2015).

[2] G. I. Japaridze and A. P. Kampf, Weak-coupling phase diagram of the extended hubbard model with correlated-hopping interaction, Phys. Rev. B **59**, 12822 (1999).

[3] T. J. Elliott and I. B. Mekhov, Engineering many-body dynamics with quantum light potentials and measurements, Phys. Rev. A **94**, 013614 (2016).

[4] F. Görg, K. Sandholzer, J. Minguzzi, R. Desbuquois, M. Messer, and T. Esslinger, Realization of density-dependent peierls phases to engineer quantized gauge fields coupled to ultracold matter, Nat. Phys. **15**, 1161 (2019).

[5] C. Schweizer, F. Grusdt, M. Berngruber, L. Barbiero, E. Demler, N. Goldman, I. Bloch, and M. Aidelsburger, Floquet approach to $\mathbb{Z}_2$ lattice gauge theories with ultracold atoms in optical lattices, Nat. Phys. **15**, 1168 (2019).

[6] C. V. Kraus, M. Dalmonte, M. A. Baranov, A. M. Läuchli, and P. Zoller, Majorana Edge States in Atomic Wires Coupled by Pair Hopping, Phys. Rev. Lett. **111**, 173004 (2013).

[7] T. Chanda, R. Kraus, G. Morigi, and J. Zakrzewski, Self-organized topological insulator due to cavity-mediated correlated tunneling, Quantum **5**, 501 (2021).

[8] R. Ma, M. E. Tai, P. M. Preiss, W. S. Bakr, J. Simon, and M. Greiner, Photon-Assisted Tunneling in a Biased Strongly Correlated Bose Gas, Phys. Rev. Lett. **107**, 095301 (2011).

[9] F. Meinert, M. J. Mark, K. Lauber, A. J. Daley, and H.-C. Nägerl, Floquet Engineering of Correlated Tunneling in the Bose-Hubbard Model with Ultracold Atoms, Phys. Rev. Lett. **116**, 205301 (2016).

[10] W. Xu, W. Morong, H.-Y. Hui, V. W. Scarola, and B. DeMarco, Correlated spin-flip tunneling in a fermi lattice gas, Phys. Rev. A **98**, 023623 (2018).

[11] L. W. Clark, B. M. Anderson, L. Feng, A. Gaj, K. Levin, and C. Chin, Observation of Density-Dependent Gauge Fields in a Bose-Einstein Condensate Based on Micromotion Control in a Shaken Two-Dimensional Lattice, Phys. Rev. Lett. **121**, 030402 (2018).

[12] S. Baier, M. J. Mark, D. Petter, K. Aikawa, L. Chomaz, Z. Cai, M. Baranov, P. Zoller, and F. Ferlaino, Extended bose-hubbard models with ultracold magnetic atoms, Science **352**, 201 (2016).

[13] F. Mivehvar, F. Piazza, T. Donner, and H. Ritsch, Cavity qed with quantum gases: New paradigms in many-body physics, Adv. Phys. **70**, 1 (2021).

[14] K. Baumann, C. Guerlin, F. Brennecke, and T. Esslinger, Dicke quantum phase transition with a superfluid gas in an optical cavity, Nature (London) **464**, 1301 (2010).

[15] J. Klinder, H. Keßler, M. R. Bakhtiari, M. Thorwart, and A. Hemmerich, Observation of a Superradiant Mott Insulator in the Dicke-Hubbard Model, Phys. Rev. Lett. **115**, 230403 (2015).

[16] M. A. Norcia, R. J. Lewis-Swan, J. R. Cline, B. Zhu, A. M. Rey, and J. K. Thompson, Cavity-mediated collective spin-exchange interactions in a strontium superradiant laser, Science **361**, 259 (2018).

[17] E. J. Davis, G. Bentsen, L. Homeier, T. Li, and M. H. Schleier-Smith, Photon-Mediated Spin-Exchange Dynamics of Spin-1 Atoms, Phys. Rev. Lett. **122**, 010405 (2019).

[18] J. A. Muniz, D. Barberena, R. J. Lewis-Swan, D. J. Young, J. R. K. Cline, A. M. Rey, and J. K. Thompson, Exploring dynamical phase transitions with cold atoms in an optical cavity, Nature (London) **580**, 602 (2020).

[19] S. C. Schuster, P. Wolf, S. Ostermann, S. Slama, and C. Zimmermann, Supersolid Properties of a Bose-Einstein Condensate in a Ring Resonator, Phys. Rev. Lett. **124**, 143602 (2020).

[20] X. Zhang, Y. Chen, Z. Wu, J. Wang, J. Fan, S. Deng, and H. Wu, Observation of a superradiant quantum phase transition in an intracavity degenerate fermi gas, Science **373**, 1359 (2021).

[21] Y. Guo, R. M. Kroeze, B. P. Marsh, S. Gopalakrishnan, J. Keeling, and B. L. Lev, An optical lattice with sound, Nature (London) **599**, 211 (2021).

[22] A. Periwal, E. S. Cooper, P. Kunkel, J. F. Wienand, E. J. Davis, and M. Schleier-Smith, Programmable interactions and emergent geometry in an array of atom clouds, Nature (London) **600**, 630 (2021).

[23] H. Konishi, K. Roux, V. Helson, and J.-P. Brantut, Universal pair polaritons in a strongly interacting fermi gas, Nature (London) **596**, 509 (2021).

[24] R. Rosa-Medina, F. Ferri, F. Finger, N. Dogra, K. Kroeger, R. Lin, R. Chitra, T. Donner, and T. Esslinger, Observing Dynamical Currents in a Non-Hermitian Momentum Lattice, Phys. Rev. Lett. **128**, 143602 (2022).

[25] A. Sondberg Sørensen and K. Mølmer, Entangling atoms in bad cavities, Phys. Rev. A **66**, 022314 (2002).

[26] A. N. Pyrkov and T. Byrnes, Entanglement generation in quantum networks of bose–einstein condensates, New J. Phys. **15**, 093019 (2013).

[27] A. Celi, P. Massignan, J. Ruseckas, N. Goldman, I. B. Spielman, G. Juzeliūnas, and M. Lewenstein, Synthetic Gauge Fields in Synthetic Dimensions, Phys. Rev. Lett. **112**, 043001 (2014).

[28] T. Ozawa and H. M. Price, Topological quantum matter in synthetic dimensions, Nat. Rev. Phys. **1**, 349 (2019).

[29] M. Mancini, G. Pagano, G. Cappellini, L. Livi, M. Rider, J. Catani, C. Sias, P. Zoller, M. Inguscio, M. Dalmonte, and L. Fallani, Observation of chiral edge states with neutral fermions in synthetic hall ribbons, Science **349**, 1510 (2015).

[30] B. K. Stuhl, H.-I. Lu, L. M. Aycock, D. Genkina, and I. B. Spielman, Visualizing edge states with an atomic bose gas in the quantum hall regime, Science **349**, 1514 (2015).

[31] S. Kolkowitz, S. L. Bromley, T. Bothwell, M. L. Wall, G. E. Marti, A. P. Koller, X. Zhang, A. M. Rey, and J. Ye, Spin–orbit-coupled fermions in an optical lattice clock, Nature (London) **542**, 66 (2017).

[32] T. Chalopin, T. Satoor, A. Evrard, V. Makhalov, J. Dalibard, R. Lopes, and S. Nascimbene, Probing chiral edge dynamics and bulk topology of a synthetic hall system, Nat. Phys. **16**, 1017 (2020).

[33] T.-W. Zhou, G. Cappellini, D. Tusi, L. Franchi, J. Parravicini, C. Repellin, S. Greschner, M. Inguscio, T. Giamarchi, M. Filippone, J. Catani, and L. Fallani, Observation of universal hall response in strongly interacting fermions, arXiv:2205.13567.

[34] See Supplemental Material at http://link.aps.org/supplemental/10.1103/PhysRevResearch.5.L022034 for details of adiabatic elimination, undepleted pump approximation, numerical results for dynamical phase transition and experimental considerations (includes Refs. [16,18,35,44,46]).

[35] A. Piñeiro Orioli, J. K. Thompson, and A. M. Rey, Emergent Dark States from Superradiant Dynamics in Multilevel Atoms in a Cavity, Phys. Rev. X **12**, 011054 (2022).

[36] L. Pezzè, A. Smerzi, M. K. Oberthaler, R. Schmied, and P. Treutlein, Quantum metrology with nonclassical states of atomic ensembles, Rev. Mod. Phys. **90**, 035005 (2018).

[37] O. Katz, M. Cetina, and C. Monroe, *n*-Body Interactions Between Trapped Ion Qubits Via Spin-Dependent Squeezing, Phys. Rev. Lett. **129**, 063603 (2022).

[38] H.-X. Yang, T. Tian, Y.-B. Yang, L.-Y. Qiu, H.-Y. Liang, A.-J. Chu, C. B. Dağ, Y. Xu, Y. Liu, and L.-M. Duan, Observation of dynamical quantum phase transitions in a spinor condensate, Phys. Rev. A **100**, 013622 (2019).

[39] M. O. Scully and M. S. Zubairy, *Quantum Optics* (Cambridge University Press, Cambridge, 1997).

[40] J. Kitzinger, M. Chaudhary, M. Kondappan, V. Ivannikov, and T. Byrnes, Two-axis two-spin squeezed states, Phys. Rev. Res. **2**, 033504 (2020).

[41] M. Cheneau, P. Barmettler, D. Poletti, M. Endres, P. Schauß, T. Fukuhara, C. Gross, I. Bloch, C. Kollath, and S. Kuhr, Light-cone-like spreading of correlations in a quantum many-body system, Nature (London) **481**, 484 (2012).

[42] P. Jurcevic, B. P. Lanyon, P. Hauke, C. Hempel, P. Zoller, R. Blatt, and C. F. Roos, Quasiparticle engineering and entanglement propagation in a quantum many-body system, Nature (London) **511**, 202 (2014).

[43] P. Richerme, Z.-X. Gong, A. Lee, C. Senko, J. Smith, M. Foss-Feig, S. Michalakis, A. V. Gorshkov, and C. Monroe, Non-local propagation of correlations in quantum systems with long-range interactions, Nature (London) **511**, 198 (2014).

[44] M. A. Norcia, J. R. K. Cline, J. A. Muniz, J. M. Robinson, R. B. Hutson, A. Goban, G. E. Marti, J. Ye, and J. K. Thompson, Frequency Measurements of Superradiance from the Strontium Clock Transition, Phys. Rev. X **8**, 021036 (2018).

[45] R. Belyansky, P. Bienias, Y. A. Kharkov, A. V. Gorshkov, and B. Swingle, Minimal Model for Fast Scrambling, Phys. Rev. Lett. **125**, 130601 (2020).

[46] M. M. Boyd, T. Zelevinsky, A. D. Ludlow, S. Blatt, T. Zanon-Willette, S. M. Foreman, and J. Ye, Nuclear spin effects in optical lattice clocks, Phys. Rev. A **76**, 022510 (2007).